High-Capacity, Low-Power Axial AMB for Flywheel Energy Storage Systems: Design, Analysis, and Validation

Shih-Ying CHIANG*, Chao-Yun CHEN*, and Kuo-Shu HUNG*
*Industrial Technology Research Institute, Taiwan, R.O.C.
195, Sec. 4, Chung Hsing Rd., Chutung, Hsinchu, 310401, Taiwan, R.O.C.
E-mail: PaulChiang@itri.org.tw

Abstract
Flywheel Energy Storage System (FESS) has the characteristics of fast charging and discharging, suitable for integration with renewable energy to stabilize the grid. The capacity of a Flywheel Energy Storage System (FESS) is directly proportional to its rotor mass. Consequently, the higher the load its axial bearing can support, the greater the flywheel energy storage capacity it can achieve. When solely relying on electromagnets as suspension actuators, Active Magnetic Bearings (AMBs) face a significant limitation in their application to FESS due to substantial energy losses. This study presents a novel axial AMB that leverages permanent magnet forces to counterbalance rotor weight. Through a combination of theoretical analysis, simulation, and experimental validation, the axial AMB's structure is proven to exhibit excellent linear characteristics. Our experiments showed that the axial AMB operates effectively with a Linear Quadratic Regulator (LQR) controller. Notably, the control current decreases linearly as the supported axial weight increases. Importantly, when the output axial force equals the flywheel's weight, the system achieves a notably low current consumption. As a crucial component bearing the flywheel's load, the axial AMB's linear relationship between axial output and control current is vital for controller robustness. This study proposes an axial AMB exhibiting linearity and low power loss, aiming to make a pivotal contribution to the development of magnetic suspension flywheel systems.

Keywords : Flywheel Energy Storage System, Active Magnetic Bearing, Linear Quadratic Regulator, Permanent Magnet Biased AMB, Turbo Molecular Pump, Finite Element Analysis

1. Introduction

As renewable energy flourishes, the challenge of harnessing its intermittent electricity has become a global priority. Unlike cell stacks, which convert chemical energy into electricity, Flywheel Energy Storage Systems (FESS) leverage the reversible conversion between mechanical and electrical energy, with the process being almost entirely lossless except for some friction losses. This characteristic gives FESS a longer lifespan and lower maintenance costs compared to cell stacks. However, the impact of friction makes FESS less suitable for long-term electricity storage. The integration of Active Magnetic Bearings (AMBs) into FESS significantly reduces friction losses, enhancing overall efficiency. Beyond the initial frictional resistance, the predominant loss in FESS is electrical energy consumption. Notably, while a heavier flywheel stores more rotational energy, it also demands a stronger bearing load capacity, leading to increased energy losses. Enhancing the energy-saving capabilities of AMBs can prolong the availability of stored kinetic energy, potentially making FESS a viable alternative to traditional battery stacks.

The conventional axial AMB system, as depicted in Fig. 1, utilizes two pairs of coils positioned on either side of the thrust disk. By modulating the exciting currents through these coils, the system exerts control over the direction of the resultant magnetic force acting upon the disk. An integrated displacement sensor, continuously monitoring the disk's axial displacement, triggers corrective actions. For instance, if the disk deviates downward, the control system compensates by adjusting the coil currents: it increases the current in the upper coil while decreasing it in the lower coil, thereby enhancing the resultant magnetic force upwards to correct the disk's position. This process is fully reversible, adjusting currents in the opposite manner to correct upward deviations. It is evident that, even in the absence of external forces on the disk, the controller must still output a balanced current to the two coils, referred to as the base current. This current is necessary to provide the requisite stiffness for the AMB. To enhance the axial AMB's output, some researchers have

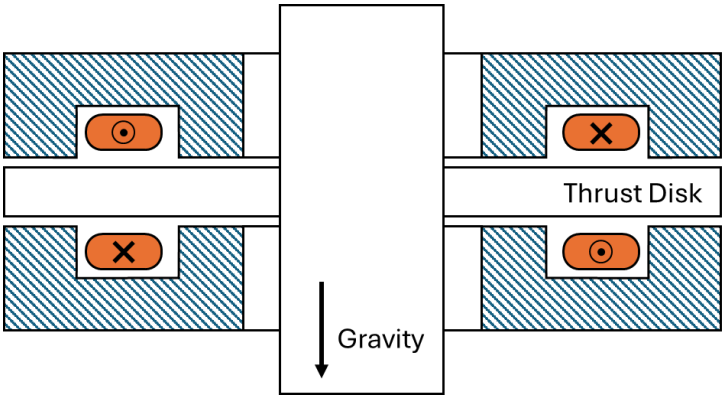

Fig. 1 A conventional axial AMB illustration features a pair of electromagnets positioned on the opposing faces of a thrust disk. The electromagnet coils generate magnetic fields in opposite directions. By applying differential currents, a net magnetic force is produced, acting along the gravity direction to support the thrust disk.

proposed replacing traditional dual-sided electromagnets with a single-sided electromagnetic configuration (Kanematsu et al., 2014). This architecture is particularly suited for applications where the rotation axis is parallel to the gravitational direction, such as in turbo molecular pumps (TMPs) and FESS. Notably, this design eliminates the need for a base current, allowing the entire electrical power to be utilized for supporting the axial load. However, as the load increases, the output current rises non-linearly, making the design of its controller more challenging. In addition to electromagnetic coils, incorporating permanent magnets as an auxiliary component is expected to further reduce the required input current. However, the uncontrollable nature of permanent magnets inevitably complicates the design of the controller. Typical permanent magnet biased AMB technologies mitigate this by using geometric design to limit the magnetic flux of permanent magnets, thereby decoupling their magnetic field from that of the excited coils (Filatov et al.,2016). This concept inspired the core idea of our research: utilizing permanent magnets to support the rotor's weight and electromagnetic coils for fine adjustments to achieve magnetic levitation. The paramount challenge lies in simplifying the nonlinear physical behavior to design a linear, high-performance axial AMB. This study first employs analytical methods for theoretical derivation, followed by numerical simulation and experimental validation to verify the design concept of the axial AMB.

2. Design of Axial AMBs

2.1 Axial AMB structure and its design limitations

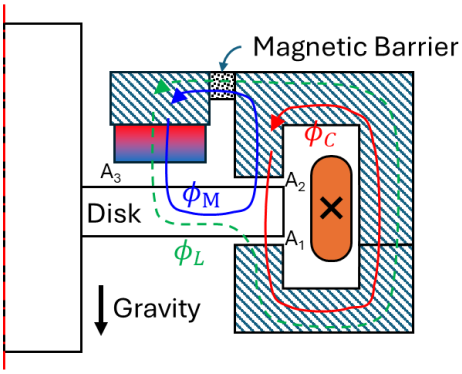

Fig. 2 A novel axial AMB design incorporates two key magnetic flux components: a permanent magnetic flux (blue solid lines) and an exciting magnetic flux (red solid lines). Their interaction generates a composite leakage flux, visualized by green dashed lines. The configuration features three distinct air-gap surfaces: one between the lower magnetic yoke and disk (area A_1), another between the upper magnetic yoke and disk (area A_2), and a third defined by the permanent magnet and disk (area A_3). Notably, the permanent magnetic flux is constrained by an integrated magnetic barrier structure to maintain saturation.

Inspired by the research conducted by Filatov et al., we have devised a novel axial AMB structure, as illustrated in Fig. 2. The fixed component of this bearing consists of two magnetic yokes, upper and lower. The upper yoke incorporates permanent magnets, which generate a magnetic force to counteract the gravitational force on the rotor. Both upper and lower yokes enclose a coil. Upon coil excitation, a closed exciting magnetic flux is produced, sequentially traversing the upper yoke, lower yoke, air gap A_1, the disk, and air gap A_2. Meanwhile, the permanent magnets establish a permanent magnetic flux, passing through the permanent magnets, upper yoke, air gap A_2, disk, and air gap A_3. Notably, a magnetic barrier structure is integrated into the upper yoke, inducing magnetic saturation in the permanent magnet's flux path at this location. This design effectively limits the permanent magnet's flux and decouples it from the exciting magnetic flux path. In addition to the permanent and exciting magnetic fluxes, the permanent magnet and the excited coil share a common leakage flux path, which sequentially goes through the upper yoke, lower yoke, air gap A_1 air gapA_3, and back to the permanent magnet. Given the known values of the permanent magnetic flux ϕ_M, exciting magnetic flux ϕ_C, leakage flux ϕ_L, and the ratio of the areas of the three air gap surfaces ($\lambda = A_1/A_2$, $\lambda' = A_1/A_3$), an analytical solution for the resultant force on the disk can be derived (Chiang et al., 2024), as shown in Eq. (1)-(3), where μ_0 is vacuum permeability.

$$\sum F_{disk} = \frac{1}{2\mu_0 A_1}(\phi_{ctrl} + \phi_{nctrl}) \tag{1}$$

$$\phi_{ctrl} = (\lambda - 1)\phi_C{}^2 - 2(\lambda\phi_M + \phi_L)\phi_C \tag{2}$$

$$\phi_{nctrl} = (\lambda + \lambda')\phi_M{}^2 + (\lambda' - 1)\phi_L{}^2 + 2\lambda'\phi_M\phi_L \tag{3}$$

The component ϕ_{ctrl} is directly related to the exciting magnetic flux and is proportionally controlled by the control current. By setting λ to one, the nonlinear component associated with the exciting magnetic flux (and thus the control current) can be eliminated, making the output directly proportional to the excitation flux (or control current). In contrast, ϕ_{nctrl} represents the component unrelated to the exciting magnetic flux. When the permanent magnet flux becomes locally saturated due to the magnetic barrier structure, it can be considered a constant value, with the leakage flux effectively being zero. Under this condition, ϕ_{nctrl} remains a constant, unaffected by changes in the control current. Based on the aforementioned assumptions, Equation (1) can be rewritten in the form of Eq. (4), where $A_1 = A_2 = A$.

$$\sum F_{disk} = \frac{1}{\mu_0 A}\left(\frac{1+\lambda'}{2}\phi_M{}^2 - \phi_M\phi_C\right) \tag{4}$$

It is noteworthy that, in reality, the magnetic flux density of ferromagnetic materials in a saturated state is not entirely constant. Consequently, variations in the air-gap reluctance due to disk displacement will still induce changes in the permanent magnet flux. The conclusion drawn from Eq. (4) is only applicable under the condition where there is no disk displacement. Furthermore, given that air gaps A_1 and A_2 have equal areas, and assuming a control current of i_c, the air gap of g and a coil turn count of N, equation (4) can be further refined into Eq. (5). This reveals a linear relationship between the axial AMB's output and the control current, where an increase in control current corresponds to a decrease in the bearing force.

$$\sum F_{disk} = \frac{(1+\lambda')\phi_M{}^2}{2\mu_0 A} - \frac{\phi_M N}{2g} i_C \tag{5}$$

2.2 Design axial AMB by simulation

Given that the permanent magnetic flux is a function of the air gap dimensions, understanding the relationship between the axial AMB's output and the disk's position is crucial before designing the controller. However, deriving an analytical equation is challenging due to the nonlinear properties of the magnets and yokes. To address this, our study employs numerical simulation using ANSYS Maxwell 2D to establish and analyze an axisymmetric finite element model (as illustrated in Fig. 3). By systematically reducing the cross-sectional of the magnetic barrier design until the axial resultant force starts to decrease, we determine the point at which the permanent magnetic flux is effectively limited, achieving our design objective (Fig. 4). Considering the actual permanent magnetic flux's correlation with disk's displacement, the design ensures a safe margin from the critical point to guarantee that the magnetic barrier structure operates in a saturated state across the entire range of disk's displacement.

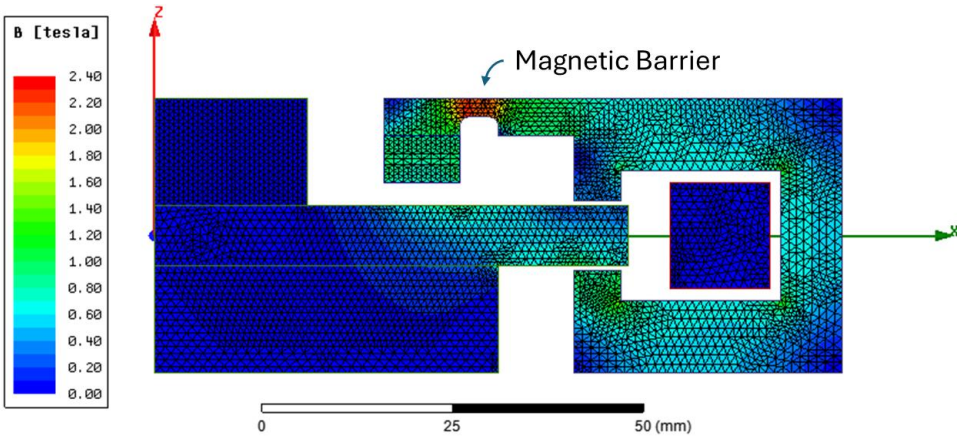

Fig. 3 The axial AMB features an axisymmetric finite element model. When a current of 2.5A is applied to its coil, the disk maintains a uniform air gap of 0.5mm from both the upper and lower magnetic bearings. Notably, an magnetic barrier structure is integrated into the upper magnetic bearing. As evidenced by the magnetic flux density map, this specific design element operates in a magnetically saturated state, thereby effectively limiting the flux of the permanent magnet.

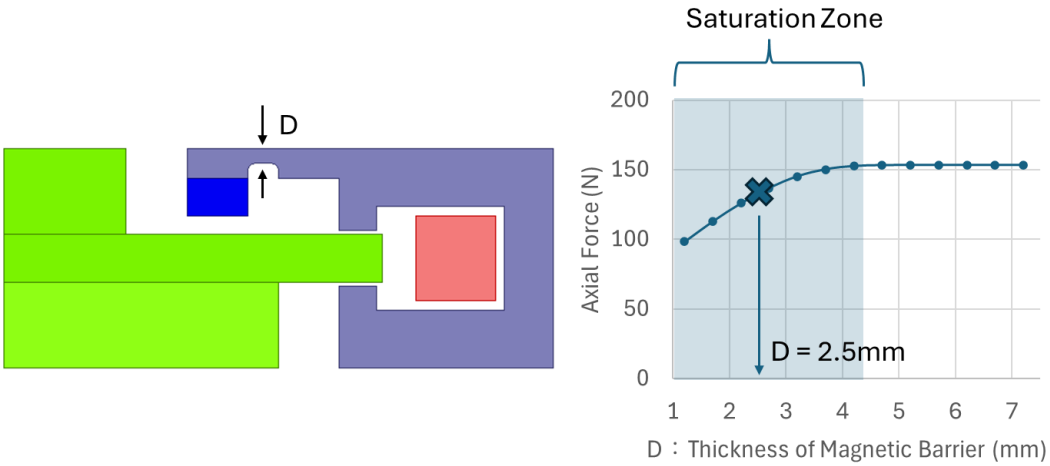

Fig. 4 A parametric analysis was conducted by increasing the thickness of the magnetic shield structure from 1.2mm to 7.2mm. The analysis revealed that the axial force exerted on the disk begins to decrease when the thickness is less than 4.2mm. This phenomenon occurs due to magnetic saturation in the magnetic barrier structure, which limits the magnetic force exerted by the axial AMB on the disk. In practical design, considering a safety margin, a thickness of 2.5mm is adopted as the design point.

The validity of the aforementioned Eq. (5) is contingent upon the magnetic flux path conforming to the specified design conditions. However, if the structural design is flawed, leading to unforeseen leakage flux phenomena, the linear relationship between the control current and the AMB output will be compromised. As illustrated in Fig. 5, when the distance between the rotor and the magnet is on the same scale as the designed air gap, significant leakage flux will occur, resulting in a nonlinear relationship between the bearing output and the control current.

After adjusting the critical geometric dimensions of the magnetic yoke (by reducing the magnetic barrier structure and eliminating the flux leakage path), a parameterized analysis was conducted focusing on two key parameters: disk displacement and control current. The disk displacement ranged from -0.2mm to 0.2mm, while the control current spanned from -3A to 3A. A scatter plot illustrating these parameters is shown in Fig. 6. Analysis revealed that the scatter plot can be effectively fitted by a plane equation, as presented in Eq. (6), where K_s and K_i represent the displacement stiffness and current stiffness, respectively. F_0 denotes the initial magnetic force exerted on the rotor when it is at the

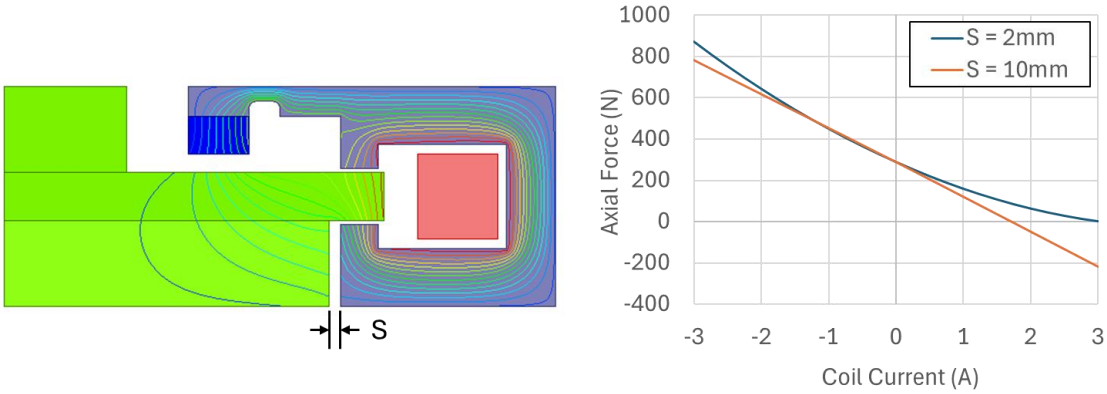

Fig. 5 When the rotor, made of soft iron material, is in close proximity to the magnetic yoke, additional leakage flux is generated. Notably, comparative analyses reveal that when the distance between the rotor and the lower magnetic yoke is reduced from 10mm to 2mm, the results exhibit a pronounced nonlinear phenomenon at the 2mm distance.

equilibrium point and no control current is applied. To minimize power consumption of the magnetic levitation flywheel system as much as possible, F_0 is designed to be equivalent to the weight of the flywheel rotor. This design enables the system to operate at a near-zero control current at the equilibrium point. Equation (6) indicates that the axial AMB's output is directly proportional to its displacement. When the disk displacement is zero, Equation (6) can simplify to Eq. (5). The validation through Eq. (6) highlights the axial AMB's excellent linear characteristic, making it directly applicable for designing linear controllers.

$$\sum F_{disk} = F_0 + K_s x - K_i i_C \tag{6}$$

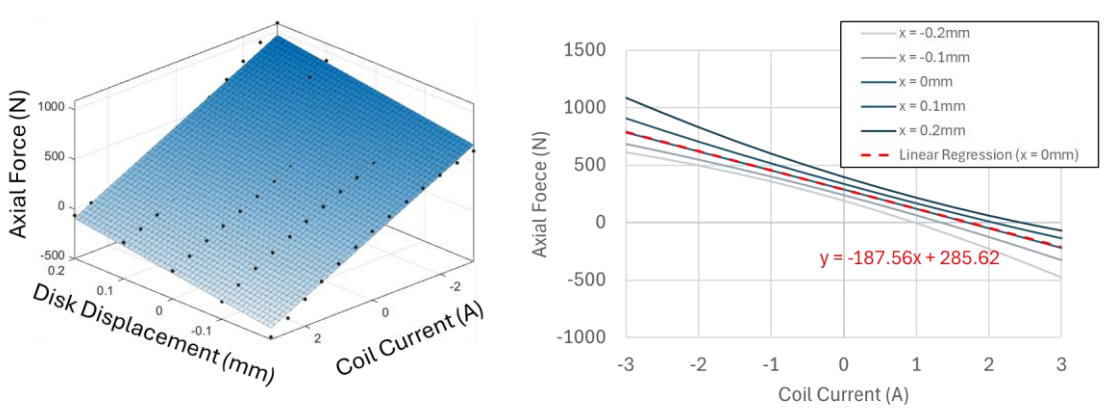

Fig. 6 A parametric analysis was conducted on the relationship between disk displacement (ranging from -0.2mm to 0.2mm) and control current (ranging from -3A to 3A). The axial force could be effectively fitted in a plane equation. Notably, when the air gaps between the disk and the upper and lower magnetic yokes were equalized, a remarkably good linear fitting result was achieved.

3. Prototype of Axial AMB

3.1 Prototype and testing equipment

Based on the results of numerical simulation analysis, a novel axial AMB's experimental model was designed, as shown in Fig. 7. This model utilizes NdFeB magnets and features a non-magnetic aluminum alloy reinforcement for the magnetic barrier structure to enhance the stiffness of the magnetic yoke. The experimental model is designed with a single degree of freedom in the axial direction, while radial displacement is constrained by a set of linear ball bearings. The combined weight of the axial bearing's disk and the shaft is 8.43 kg. Additional weight can be attached to the shaft

using counterweight plates, allowing the total weight to exceed 50 kg. An eddy current sensor (Micro-epsilon eddyNCDT 3005), boasting a 1mm measurement range, is employed to measure displacement information and is mounted near by the bottom of the disk in a location less susceptible to force-induced deformation, ensuring that the measurement point rests on a rigid foundation.

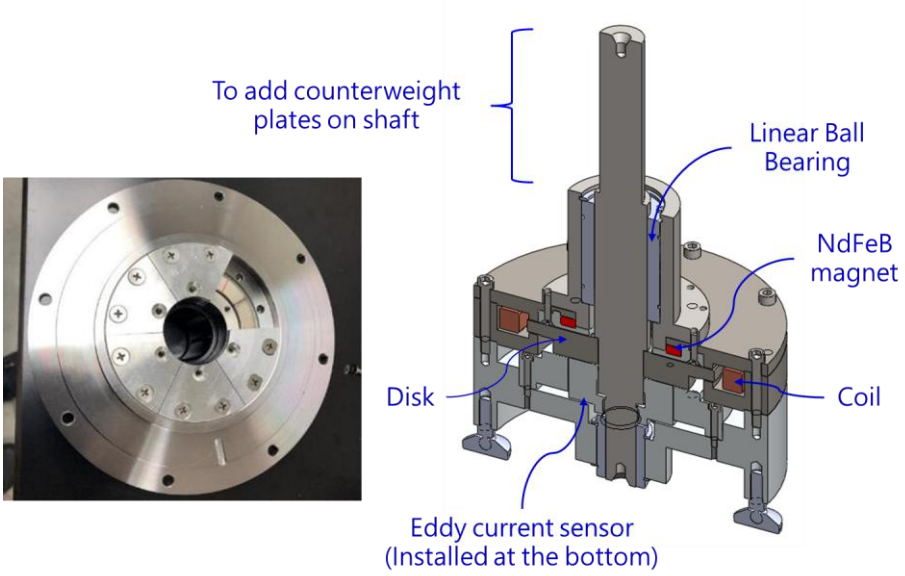

Fig. 7 The experimental model features an axisymmetric architecture, comprising six sector-shaped magnets arranged in a circular configuration and secured by aluminum alloy clamps. The counterweight plates can be added above the shaft to increase axial loading. A pair of linear bearings constrains radial movement and an eddy current sensor is mounted below the disk (not shown in the figure).

The control system's hardware foundation is built upon the Texas Instruments C2000 Digital Signal Processor (DSP). The drive circuit is configured in a full-bridge topology, facilitating a controlled current range spanning from -3A to 3A. For the current control loop, a Proportional-Integral (PI) controller is utilized, designed to operate at a control frequency of 30kHz. In contrast, the position control loop employs a Linear Quadratic Regulator (LQR) controller (Wang and Cuan, 2022), operating at a lower control frequency of 5kHz. Equation (7) reveals the state equation of the axial AMB, where m is mass of rotor. Evidently, once the displacement stiffness K_s and current stiffness K_i of the bearing are obtained through simulation, a corresponding controller can be designed based on this state equation.

$$\begin{Bmatrix} \dot{x} \\ \ddot{x} \end{Bmatrix} = \begin{bmatrix} 0 & 1 \\ \frac{K_s}{m} & 0 \end{bmatrix} \begin{Bmatrix} x \\ \dot{x} \end{Bmatrix} + \begin{Bmatrix} 0 \\ -\frac{K_i}{m} \end{Bmatrix} i_c \tag{7}$$

3.2 Experimental results

The static suspension experiment utilized the same controller to incrementally increase the load from 10Kg to 50Kg. The steady-state coil current readings were observed and recorded at the equilibrium position ($x = 0$), with results shown in Fig. 8. The experiment revealed that the output of the axial AMB and its control current relationship could be accurately fitted with a linear equation. The slope of this line, representing the axial AMB's current stiffness, was approximately $-139.7\ N/A$, which is about 25% lower than the simulated value. This discrepancy is primarily attributed to the simulation not accounting for high-frequency harmonics induced by the actual power switching component, which were not mitigated in the experimental device (e.g., no silicon steel sheets were used to suppress eddy currents). Consequently, significant eddy current losses in the magnetic yoke, leading to a lower current stiffness value than estimated, were anticipated. However, a comparison between simulated and experimental fitting equations showed that the initial magnetic force (F_0) was remarkably close, validating that Finite Element Analysis (FEA) results can accurately design rotor loads at the FESS design point, where eddy current losses are not a consideration. Furthermore, a static suspension test with a 20Kg load demonstrated a steady-state current of only 0.117A, confirming that this Axial AMB can stably control the disk position at near-zero current.

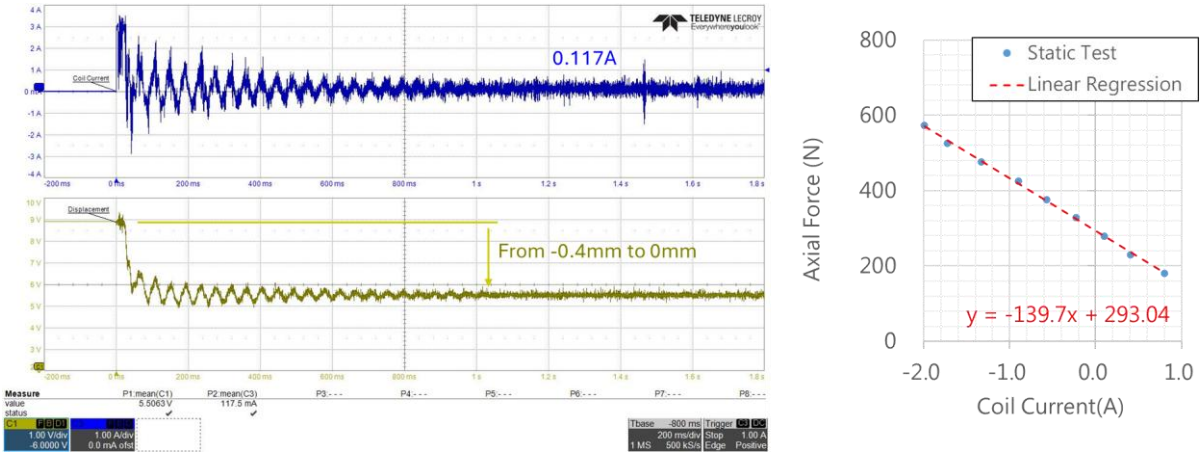

Fig. 8 The left image depicts the transient response at the 0mm equilibrium position, initiated from a -0.4mm offset with a 20Kg counterweight plate attached. The oscilloscope records both the coil current (in blue) and the disk displacement (in brown). This setup captures the axial load and the corresponding steady-state coil current. The right figure presents the results of static tests conducted with varying weights, demonstrating a linear relationship between the axial load and the control current.

4. Conclusion

This study proposes an axial AMB architecture that leverages permanent magnets to balance and support the rotor load, thereby meeting the objectives of low current and high load capacity. Analysis revealed that to establish a linear relationship between the axial AMB's output and the control current, two conditions must be simultaneously satisfied: the air-gap areas between the upper/lower magnetic yokes and the disk must be equal, and the permanent magnetic flux must pass through a magnetic barrier structure while maintaining a saturated state.

Through finite element analysis, parametric study on disk displacement and control current were conducted, leading to the determination of the axial AMB's displacement stiffness and current stiffness. This enabled the design of an LQR controller.

Under various load conditions, static suspension experiments were performed on the Axial AMB, validating the linear relationship between the control current and axial output. Although neglecting eddy current losses resulted in an overestimation of current stiffness, the results demonstrated the controller's robustness. The initial magnetic force values obtained from simulation analysis proved sufficiently accurate for direct application to the flywheel rotor's load. The proposed Axial AMB, characterized by its high load capacity and low loss, is particularly suited for applications requiring stable support of large loads, such as flywheel energy storage systems.

5. Acknowledgments

The authors would like to thank the Energy Administration, Ministry of Economic Affairs, Taiwan, R.O.C., for supporting this research.

References

Chiang S. Y., Chen C. Y. and Hung K. S., Design of Axial Active Magnetic Bearing with High Load Capacity for Low Pressure Centrifugal Chiller, International Compressor Engineering Conference. (2024) Paper 2820.

Filatov, A., Hawkins, L. and McMullen, P. Homopolar Permanent-magnet-biased actuators and their application in rotational active magnetic bearing systems., Actuators, 5(4), 26. (2016)

Kanematsu H., Wakui S. and Nakamura Y., Analysis and control of one-axis active magnetic bearing using single side electromagnetic drive, 2014 IEEE/ASME International Conference on Advanced Intelligent Mechatronics, Besacon, France, (2014), pp. 781-787

Wang L. P., Cuan. R. P., State Feedback Control and Kalman Filtering with MATLAB/Simulink Tutorials, John Wiley & Sons, (2022), pp. 217-218.